Numerical investigation of rotor-bearing systems with fractional derivative material damping models

Gregor ÜBERWIMMER [ID]*, Georg QUINZ, Michael KLANNER [ID], and Katrin ELLERMANN

Graz University of Technology, Institute of Mechanics, Kopernikusgasse 24/IV, 8010 Graz, Austria

Abstract. The increasing demand for high-speed rotor-bearing systems results in the application of complex materials, which allow for a better control of the vibrational characteristics. This paper presents a model of a rotor including viscoelastic materials and valid up to high spin speeds. Regarding the destabilization of rotor-bearing systems, two main effects have to be investigated, which are strongly related to the associated internal and external damping of the rotor. For this reason, the internal material damping is modeled using fractional time derivatives, which can represent a large class of viscoelastic materials over a wide frequency range. In this paper, the Numerical Assembly Technique (NAT) is extended for the rotating viscoelastic Timoshenko beam with fractional derivative damping. An efficient and accurate simulation of the proposed rotor-bearing model is achieved. Several numerical examples are presented and the influence of internal damping on the rotor-bearing system is investigated and compared to classical damping models.

Key words: Numerical Assembly Technique; rotor-bearing system; steady-state harmonic vibration; unbalance response; fractional derivative damping model.

1. INTRODUCTION

Accurate knowledge of the dynamic behaviour of a rotating machine is necessary in the design process, and therefore, the focus on the material model is gaining more importance due to the application of complicated materials in rotors. In this paper, different material models are compared and the dynamic behaviour of the rotor under the influence of internal damping is investigated.

For various materials different material damping models exist. In this work, the material is described by fractional time derivatives, which were first introduced by Nutting [2] in a viscoelastic deformation law. This fractional material model has been modified and validated by several authors, e.g. [3], and describes materials in a wide frequency range [3].

Several beam theories are available to model a structure, where two dimensions are significantly smaller than the third one, e.g. the Euler-Bernoulli beam or the Timoshenko beam theory. Labuschagne *et al.* [4] compared the linear beam theories and depicted that the Timoshenko beam theory leads to better results, particulary for higher modes, as compared to the Euler-Bernoulli beam theory. Also, Ruge and Birk [5] outlined that the Timoshenko beam theory delivers physically more realistic results. Additionally, Tamraker and Mittal [6] validated with an experiment the importance of the Timoshenko beam theory for predicting the dynamic performance of a rotor. To solve the resulting mathematical problem, several numerical methods can be utilized. The most common approach is the Fi-

nite Element Method (FEM). For an analytical description and solution of the problem, the Transfer Matrix Method (TMM) is often applied.

Zorzi and Nelson [7] considered internal viscous and hysteretic damping in their extension of the linear finite element concept for evaluating the stability of a damped rotor. For describing a rotor, internal and external damping plays a major role. Genta [8] clarified the correct understanding of the stability of hysteretic (internal) damping of rotating elements stating that the system stays stable for subcritical speeds even with internal damping. Baumann *et al.* [9] investigated the stability of the rotor vibration with internal and external damping and showed the stability limits for different material models. Several authors improved the accuracy of the solution of FEM by considering effects, e.g. rotary inertia, gyroscopic moment, shear effects, and axial load [10, 11].

For calculating the critical speeds and the unbalance response of the system, TMM can be applied. Prohl [12] first introduced the TMM to rotor-bearing systems. Several authors [13, 14] extended TMM by including, e.g. gyroscopic effects, internal friction, aerodynamic cross-coupling forces, tangential torque, and distributed unbalance, and outlined the effectiveness of the method for the steady-state analysis of rotor-bearing systems with an unbalanced shaft.

In the literature, several other analytical methods can be found, which mitigate certain challenges arising in TMM. The higher accuracy and reduction of computational time are depicted in [15]. Furthermore, the Numerical Assembly Technique (NAT) is an efficient way of treating rotor problems. Wu and Chou [16] first introduced this method. Klanner *et al.* [1, 17] extended NAT for the two-dimensional Timoshenko beam and the rotating Rayleigh beam and presented the effi-

*e-mail: gregor.ueberwimmer@tugraz.at

G. Überwimmer, G. Quinz, M. Klanner, and K. Ellermann

ciency and accuracy of NAT. Quinz *et al.* [18–21] showed an application of NAT for the balancing of rotors.

The aim of this paper is the analytical solution of a rotating viscoelastic Timoshenko beam with occurring unbalanced discs considering a fractional derivative damping material model. In this way, NAT is extended for the rotating viscoelastic Timoshenko beam with fractional derivative damping. The newly implemented material model is compared to different other classical material models and the occurring differences in the unbalance response are shown.

2. PROBLEM DESCRIPTION AND MATHEMATICAL MODEL

A general multi-stepped rotor vibration problem with attached discs supported on anisotropic bearings is formulated and described by the Timoshenko beam theory.

2.1. General rotor-bearing system

In this section, a general multi-stepped rotor vibration problem is formulated and shown in Fig. 1. Each beam segment is modeled by the Timoshenko beam theory and external viscous damping is considered. The rotor is supported on anisotropic bearings with a constant spin speed Ω about the z-axis. The bearings are modeled by translational and rotational springs and dampers. The shaft has several circular discs with mass $m^{(i)}$,

mass moment of inertia about the x- and y-axis $\Theta_t^{(i)}$, mass moments of inertia about the z-axis $\Theta_p^{(i)}$, and an unbalance with eccentricity $\varepsilon^{(i)}$ and angular position $\beta^{(i)}$. For the rotor, the assumption of no axial loading is made.

The shaft has (N) stations, where each station represents a disc, a step, or bearing support of the rotor. The first (1) and the last (N) stations are placed at the boundaries ($z = 0$ and $z = L$). The intermediate stations (i) are located at $z = Z_i$. Between the stations, there are $M = (N) - 1$ segments with a constant circular cross-section, and homogenous material parameters. Each segment ℓ has a local coordinate system $(O_\ell, x_\ell, y_\ell, z_\ell)$ with the origin O_ℓ in the center of the circular cross-section at station (i).

2.2. Fractional derivative material damping models

The correlation between the stresses and strains is generalized to achieve a better-fitted material model for viscoelastic materials. The result is a model analysed by Bagley and Torvik [22], which describes the generalised form of the Kelvin-Voigt material model.

In the time domain, the correlation for the fractional Kelvin-Voigt model is given by

$$\sigma_{zz}(x,y,z,t) = a_{0\ell}^E \varepsilon_{zz}(x,y,z,t) + a_{1\ell}^E \frac{\partial^{\alpha_\ell^E} \varepsilon_{zz}(x,y,z,t)}{\partial t^{\alpha_\ell^E}}, \quad (1)$$
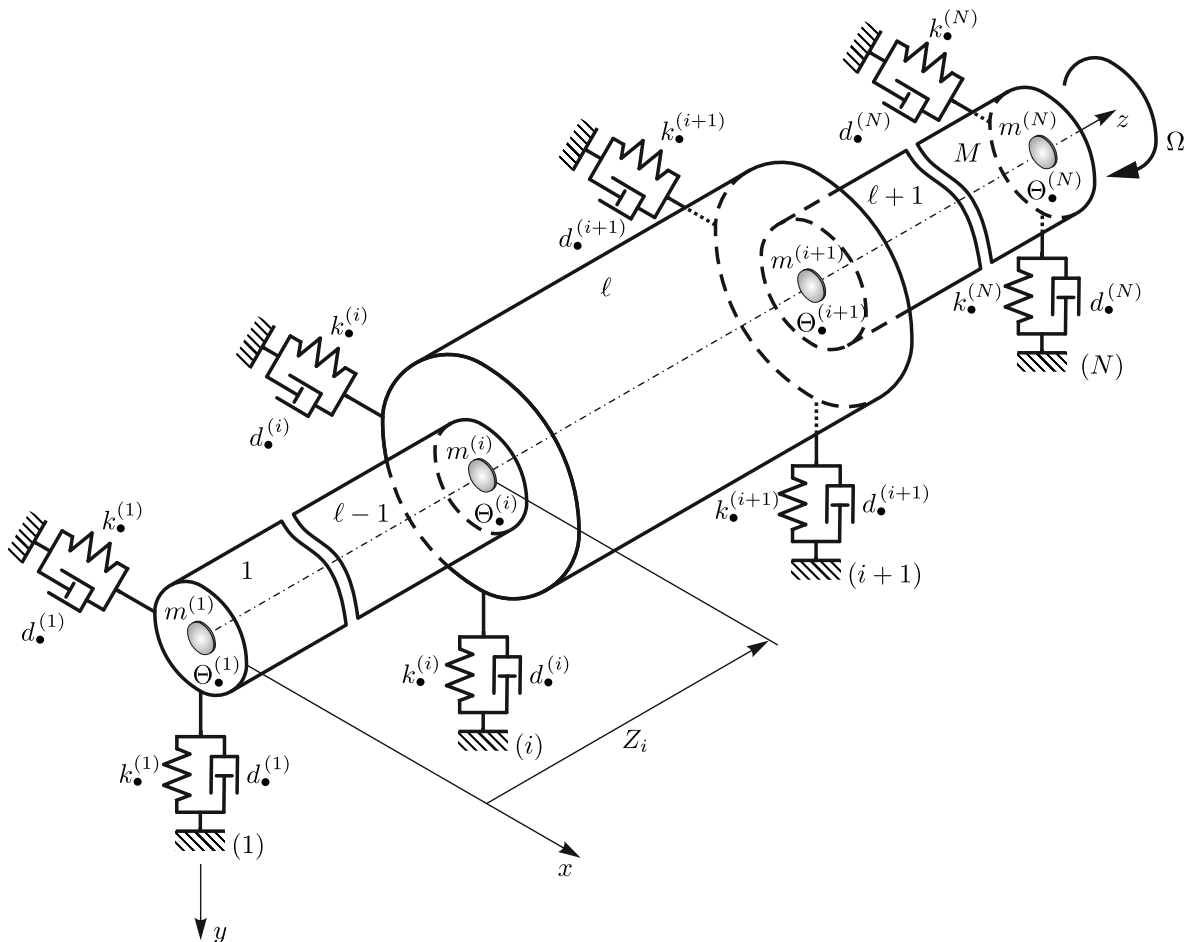
Fig. 1. General rotor problem [1]

2

Bull. Pol. Acad. Sci. Tech. Sci., vol. 71, no. 6, p. e148610, 2023

with $a_{0\ell}^E$ in N/m^2 and $a_{1\ell}^E$ in Ns$^{\alpha_\ell^E}$/m^2, positive real constants and

$$0 < \alpha_\ell^E < 1 \qquad (2)$$

due to the physical restrictions of solid materials, as Pritz showed in [3]. Therefore, the argument was made that pure viscous friction cannot be valid for a real solid material. The necessity of a "lesser extent" for solid materials due to the behaviour in the time variation of strain compared to fluids and can be mathematically expressed as $\alpha_\ell^E < 1$. With the parameter α_ℓ^E it is possible to handle the retardation and relaxation times of the material [23]. This ability results in a memory mechanism inherent in the material model [23]. $\frac{\partial^\bullet}{\partial t^\bullet}$ denotes a fractional derivative of order $\bullet$. In literature, different mathematical definitions of the fractional differential can be found. In this paper, the Riemann–Liouville fractional derivative definition has been used. It would also be possible to use the Caputo fractional definition, where the order of the ordinary derivative has been switched [24]. The Fourier transform of the Caputo operator for fractional derivatives is demonstrated in [25]. Thereby, the result of the Fourier transform is independent of the lower bound of the integral, which denotes the short-term memory parameter. This observation shows that the results remain identical for short-term and long-term memory as long as the calculations are performed in the frequency domain.

To get simplified material models certain parameters can be changed to specific values, e.g. defining $a_{1\ell}^E$ as zero, Hook's law is the result. If the parameter $\alpha_\ell^E = 1$ the Kelvin-Voigt material model is given.

2.3. Equations of motion of a rotating Timoshenko beam with mass unbalance

All beam segments are modeled by the Timoshenko beam theory. Thereby, the consideration of the shear deformation, the inertia of the cross-section for rotations about the x- and y- axis, and the gyroscopic effect are the main advantages [26]. The assumptions and the equilibrium of forces and moments of the Timoshenko beam theory can be found in [27,28].

In this work, it is assumed that the transverse displacements $u_{x\ell}(z,t)$ and $u_{y\ell}(z,t)$ and rotations $\varphi_{x\ell}(z,t)$ and $\varphi_{y\ell}(z,t)$ can be written as

$$\bullet_\ell(z,t) = \tilde{\bullet}_\ell^+(z)\, e^{j\omega t} + \tilde{\bullet}_\ell^-(z)\, e^{-j\omega t}. \qquad (3)$$

This allows for the investigation of two cases. The steady-state unbalance response, where $\omega = \Omega$, and the free vibration response with ω the general complex eigenvalues of the system. This assumption leads to decoupled complex conjugated equations of the real solution [17].

Therefore, in further investigations only the differential equations with the positive part $\bullet_\ell^+(z)$ are considered for the solution. The equations of motion for the steady-state harmonic unbalance response of a rotating Timoshenko beam are given by

$$\frac{d^2\tilde{u}_{x\ell}^+(z)}{dz^2} + \left(\bar{\omega}_\ell^2\,\bar{E}_{0\ell} - \bar{d}_{a\ell}\right)\tilde{u}_{x\ell}^+(z) - \frac{d\tilde{\varphi}_{y\ell}^+(z)}{dz}$$
$$= -\frac{\bar{\Omega}_\ell^2\,\bar{E}_{0\ell}}{2}\tilde{\varepsilon}_+(z), \qquad (4)$$

$$\frac{d^2\tilde{u}_{y\ell}^+(z)}{dz^2} + \left(\bar{\omega}_\ell^2\,\bar{E}_{0\ell} - \bar{d}_{a\ell}\right)\tilde{u}_{y\ell}^+(z) + \frac{d\tilde{\varphi}_{x\ell}^+(z)}{dz}$$
$$= \frac{j\bar{\Omega}_\ell^2\,\bar{E}_{0\ell}}{2}\tilde{\varepsilon}_+(z), \qquad (5)$$

$$\frac{d^2\tilde{\varphi}_{y\ell}^+(z)}{dz^2} + \left(\bar{\omega}_\ell^2 - \frac{1}{\bar{E}_{0\ell}\,r_\ell^2}\right)\tilde{\varphi}_{y\ell}^+(z) - j\frac{\bar{E}_{1\ell}}{\bar{E}_{0\ell}}\frac{d^2\tilde{\varphi}_{x\ell}^+(z)}{dz^2}$$
$$+ j\bar{g}_\ell\,\tilde{\varphi}_{x\ell}^+(z) + \frac{1}{\bar{E}_{0\ell}\,r_\ell^2}\frac{d\tilde{u}_{x\ell}^+(z)}{dz} = 0, \qquad (6)$$

$$\frac{d^2\tilde{\varphi}_{x\ell}^+(z)}{dz^2} + \left(\bar{\omega}_\ell^2 - \frac{1}{\bar{E}_{0\ell}\,r_\ell^2}\right)\tilde{\varphi}_{x\ell}^+(z) + j\frac{\bar{E}_{1\ell}}{\bar{E}_{0\ell}}\frac{d^2\tilde{\varphi}_{y\ell}^+(z)}{dz^2}$$
$$- j\bar{g}_\ell\,\tilde{\varphi}_{y\ell}^+(z) - \frac{1}{\bar{E}_{0\ell}\,r_\ell^2}\frac{d\tilde{u}_{y\ell}^+(z)}{dz} = 0, \qquad (7)$$

with

$$\bar{\omega}_\ell^2 = \frac{\omega^2\rho_\ell}{E_{0\ell}^\star}, \quad \bar{\Omega}_\ell^2 = \frac{\Omega^2\rho_\ell}{E_{0\ell}^\star}, \quad \bar{E}_{0\ell} = \frac{E_{0\ell}^\star}{G_\ell^\star\,k_{S_\ell}},$$
$$\bar{E}_{1\ell} = \frac{E_{1\ell}^\star}{G_\ell^\star\,k_{S_\ell}}, \quad \bar{d}_{a\ell} = \frac{j\omega\,d_{a\ell}}{G_\ell^\star\,k_{S_\ell}\,A_\ell}, \quad r_\ell^2 = \frac{I_\ell}{A_\ell},$$
$$\bar{g}_\ell = \frac{2\,\omega\,\rho_\ell\,\Omega}{E_{0\ell}^\star}, \quad G_\ell^\star = \frac{a_{0\ell}^E + a_{1\ell}^E\,(j\,\omega)^{\alpha_\ell^E}}{2(1+\nu)},$$
$$E_{0\ell}^\star = a_0^E + \frac{a_1^E}{2}\left((j(\omega-\Omega))^{\alpha_\ell^E} + (j(\omega+\Omega))^{\alpha_\ell^E}\right),$$
$$E_{1\ell}^\star = \frac{a_1^E}{2}\left((j(\omega-\Omega))^{\alpha_\ell^E} - (j(\omega+\Omega))^{\alpha_\ell^E}\right), \qquad (8)$$

and ρ_ℓ the material density, k_{S_ℓ} the shear correction factor, $d_{a\ell}$ the direction-independent external viscous damping coefficient, A_ℓ the cross-section area, I_ℓ the planar second moment of area with respect to the x- and y-axis, $\tilde{\varepsilon}_+(z) = \varepsilon(z)e^{j\beta(z)}$ the complex unbalance, and ν the Poisson's ratio. The gyroscopic effect and the material model lead to a coupling of the equations of the rotating Timoshenko beam.

2.4. Boundary and interface conditions for steady-state harmonic vibrations

To get a unique solution for the rotor problem defined by the equations (4)–(7), boundary and interface conditions are needed. For these conditions, the equilibrium of forces and moments have to be used at each station (i). Additionally, the continuity of displacement and rotation at the stations have to be considered. A detailed description of the boundary and interface conditions for a rotating Rayleigh beam with constant axial load can be found in [1]. The equilibrium of forces and moments and the continuity of displacement and rotation at each station (i) are analogous for the rotating Timoshenko beam.

3. NUMERICAL ASSEMBLY TECHNIQUE

The analytical method NAT is applied to the given problem. Thereby, the analytical solution of the governing equations (4)–(7) is used to fulfill the boundary and interface conditions. The resulting equation system has to be solved for the unknown contribution factors. In this work, it is assumed that the unbalances

Bull. Pol. Acad. Sci. Tech. Sci., vol. 71, no. 6, p. e148610, 2023

3

are concentrated at the discs and do not appear within the beam segments themselves. Therefore, only the homogeneous solutions of the governing equations are required, since $\tilde{\varepsilon}_+(z) = 0$. The unbalance forces only arise in the interface conditions. If unbalances occur within the beam segments, additional particular solutions are required to fulfill the inhomogeneous governing equations. More details on this kind of problems can be found in Klanner *et al.* [1].

3.1. Homogeneous solutions

The general homogenous solution of the equations (4)–(7) is established by setting the external unbalance $\tilde{\varepsilon}_+(z)$ to zero. The assumed solutions for the segment ℓ in the local coordinate system $(O_\ell, x_\ell, y_\ell, z_\ell)$ have the form of

$$\tilde{\bullet}^+_{h\ell}(z_\ell) = C_{\bullet\ell}\, e^{jkz_\ell}, \tag{9}$$

where $\bullet$ represents the different translations and rotations. The resulting linear equation system is given by

$$\mathbf{A}_\ell \begin{bmatrix} C_{u_x\ell} \\ C_{u_y\ell} \\ C_{\varphi_y\ell} \\ C_{\varphi_x\ell} \end{bmatrix} = \begin{bmatrix} 0 \\ 0 \\ 0 \\ 0 \end{bmatrix}, \tag{10}$$

with

$$\mathbf{A}_\ell = \begin{bmatrix} -k^2 + \bar{\omega}_\ell^2 \bar{E}_{0\ell} - \bar{d}_{a\ell} & 0 \\ 0 & -k^2 + \bar{\omega}_\ell^2 \bar{E}_{0\ell} - \bar{d}_{a\ell} \\ jk\dfrac{1}{\bar{E}_{0\ell} r_\ell^2} & 0 \\ 0 & -jk\dfrac{1}{\bar{E}_{0\ell} r_\ell^2} \\[2mm] -jk & 0 \\ 0 & jk \\ -k^2 + \bar{\omega}_\ell^2 - \dfrac{1}{\bar{E}_{0\ell} r_\ell^2} & j\left(k^2\dfrac{\bar{E}_{1\ell}}{\bar{E}_{0\ell}} + \bar{g}_\ell\right) \\ -j\left(k^2\dfrac{\bar{E}_{1\ell}}{\bar{E}_{0\ell}} + \bar{g}_\ell\right) & -k^2 + \bar{\omega}_\ell^2 - \dfrac{1}{\bar{E}_{0\ell} r_\ell^2} \end{bmatrix}, \tag{11}$$

which only has a nontrivial solution if the determinant of $\mathbf{A}_\ell$ is set to zero. The determinant of $\mathbf{A}_\ell$ can be written as a product of two polynomial functions $F(k)$ and $G(k)$, which leads to

$$k_{1,2\ell} = \pm\sqrt{\frac{1}{2}\left(-\bar{d}_{a\ell} - \bar{g}_{+\ell} + \bar{\omega}_{+\ell}^2 + \bar{E}_{0\ell}\,\bar{\omega}_\ell^2 - R_{+\ell}\right)}$$
$$= \pm\alpha_{1\ell}, \tag{12}$$

$$k_{3,4\ell} = \pm\sqrt{\frac{1}{2}\left(-\bar{d}_{a\ell} - \bar{g}_{+\ell} + \bar{\omega}_{+\ell}^2 + \bar{E}_{0\ell}\,\bar{\omega}_\ell^2 + R_{+\ell}\right)}$$
$$= \pm\alpha_{2\ell}, \tag{13}$$

$$k_{5,6\ell} = \pm\sqrt{\frac{1}{2}\left(-\bar{d}_{a\ell} + \bar{g}_{-\ell} + \bar{\omega}_{-\ell}^2 + \bar{E}_{0\ell}\,\bar{\omega}_\ell^2 - R_{-\ell}\right)}$$
$$= \pm\alpha_{3\ell}, \tag{14}$$

$$k_{7,8\ell} = \pm\sqrt{\frac{1}{2}\left(-\bar{d}_{a\ell} + \bar{g}_{-\ell} + \bar{\omega}_{-\ell}^2 + \bar{E}_{0\ell}\,\bar{\omega}_\ell^2 + R_{-\ell}\right)}$$
$$= \pm\alpha_{4\ell}, \tag{15}$$

with

$$R_{\pm\ell} = \sqrt{-\frac{4\bar{d}_{a\ell}}{\bar{E}_{\pm\ell} r_\ell^2} + \frac{4\bar{\omega}_{\pm\ell}^2}{r_\ell^2} + \left(\bar{d}_{a\ell} \mp \bar{g}_{\pm\ell} + \bar{\omega}_{\pm\ell}^2 - \bar{E}_{0\ell}\bar{\omega}_\ell^2\right)^2}, \tag{16}$$

and

$$\bar{\omega}_{\pm\ell}^2 = \frac{\omega^2 \rho_\ell}{E_{\pm\ell}^\star}, \quad \bar{E}_{\pm\ell} = \frac{E_{\pm\ell}^\star}{G_\ell^\star k_{S_\ell}}, \quad \bar{g}_{\pm\ell} = \frac{2\,\omega\,\rho_\ell\,\Omega}{E_{\pm\ell}^\star},$$
$$E_{\pm\ell}^\star = a_{0\ell}^E + a_{1\ell}^E\,(j\,(\omega \mp \Omega))^{\alpha_\ell^E}. \tag{17}$$

The roots of $F(k)$ are $\pm\alpha_{1,2\ell}$, where $\alpha_{1,2\ell}$ are the complex roots with a positive imaginary part ($\Im\{k_{\bullet\ell}\} > 0$) and the roots of $G(k)$ are $\pm\alpha_{3,4\ell}$, where $\alpha_{3,4\ell}$ are the complex roots with a positive imaginary part ($\Im\{k_{\bullet\ell}\} > 0$).

The constants $C_{u_x\ell}, C_{u_y\ell}, C_{\varphi_y\ell}$ and $C_{\varphi_x\ell}$ are not independent. The constants for the roots $\pm\alpha_{1,2\ell}$ are given by

$$C_{u_y\ell} = -jC_{u_x\ell}, \quad C_{\varphi_x\ell} = jC_{\varphi_y\ell},$$
$$C_{\varphi_y\ell} = j\frac{\alpha_{\bullet\ell}^2 - \bar{\omega}_\ell^2\bar{E}_{0\ell} + \bar{d}_{a\ell}}{\alpha_{\bullet\ell}} C_{u_x\ell}, \tag{18}$$

and for the roots $\pm\alpha_{3,4\ell}$ are described by

$$C_{u_y\ell} = jC_{u_x\ell}, \quad C_{\varphi_x\ell} = -jC_{\varphi_y\ell},$$
$$C_{\varphi_y\ell} = j\frac{\alpha_{\bullet\ell}^2 - \bar{\omega}_\ell^2\bar{E}_{0\ell} + \bar{d}_{a\ell}}{\alpha_{\bullet\ell}} C_{u_x\ell}. \tag{19}$$

The solution of the homogenous differential equation allows for the computation of the shear force and the bending moment and therefore, for the description of the whole state of the shaft. The state variables and the arbitrary constants are gathered in column vectors

$$\tilde{\mathbf{x}}^+_{h\ell}(z_\ell) = \Big[\tilde{u}^+_{hx\ell}(z_\ell), \tilde{u}^+_{hy\ell}(z_\ell), \tilde{\varphi}^+_{hy\ell}(z_\ell), \tilde{\varphi}^+_{hx\ell}(z_\ell),$$
$$\tilde{M}^+_{hy\ell}(z_\ell), \tilde{M}^+_{hx\ell}(z_\ell), \tilde{Q}^+_{hx\ell}(z_\ell), \tilde{Q}^+_{hy\ell}(z_\ell)\Big]^T, \tag{20}$$

and

$$\mathbf{c}_\ell = [c_{1\ell},\ c_{2\ell},\ c_{3\ell},\ c_{4\ell},\ c_{5\ell},\ c_{6\ell},\ c_{7\ell},\ c_{8\ell}]^T. \tag{21}$$

The upper index $\bullet^T$ marks the transpose of a vector or matrix. Finally, this leads to a matrix equation, which represents the general homogenous solution and is given by

$$\tilde{\mathbf{x}}^+_{h\ell}(z_\ell) = \mathbf{B}_\ell(z_\ell)\,\mathbf{c}_\ell, \tag{22}$$

4

Bull. Pol. Acad. Sci. Tech. Sci., vol. 71, no. 6, p. e148610, 2023

with the state variable matrix

$$\mathbf{B}_\ell(z_\ell) =$$

$$
\begin{bmatrix}
E_1^+ & E_1^- & E_2^+ & E_2^- \\
-\mathrm{j}E_1^+ & -\mathrm{j}E_1^- & -\mathrm{j}E_2^+ & -\mathrm{j}E_2^- \\
k_{\varphi 1\ell}E_1^+ & -k_{\varphi 1\ell}E_1^- & k_{\varphi 2\ell}E_2^+ & -k_{\varphi 2\ell}E_2^- \\
\mathrm{j}k_{\varphi 1\ell}E_1^+ & -\mathrm{j}k_{\varphi 1\ell}E_1^- & \mathrm{j}k_{\varphi 2\ell}E_2^+ & -\mathrm{j}k_{\varphi 2\ell}E_2^- \\
-k_{M1\ell}^+E_1^+ & -k_{M1\ell}^-E_1^- & -k_{M2\ell}^+E_2^+ & -k_{M2\ell}^-E_2^- \\
-\mathrm{j}k_{M1\ell}^+E_1^+ & -\mathrm{j}k_{M1\ell}^-E_1^- & -\mathrm{j}k_{M2\ell}^+E_2^+ & -\mathrm{j}k_{M2\ell}^-E_2^- \\
-k_{Q1\ell}E_1^+ & k_{Q1\ell}E_1^- & -k_{Q2\ell}E_2^+ & k_{Q2\ell}E_2^- \\
\mathrm{j}k_{Q1\ell}E_1^+ & -\mathrm{j}k_{Q1\ell}E_1^- & \mathrm{j}k_{Q2\ell}E_2^+ & -\mathrm{j}k_{Q2\ell}E_2^-
\end{bmatrix}
$$

$$
\begin{bmatrix}
E_3^+ & E_3^- & E_4^+ & E_4^- \\
\mathrm{j}E_3^+ & \mathrm{j}E_3^- & \mathrm{j}E_4^+ & \mathrm{j}E_4^- \\
k_{\varphi 3\ell}E_3^+ & -k_{\varphi 3\ell}E_3^- & k_{\varphi 4\ell}E_4^+ & -k_{\varphi 4\ell}E_4^- \\
-\mathrm{j}k_{\varphi 3\ell}E_3^+ & \mathrm{j}k_{\varphi 3\ell}E_3^- & -\mathrm{j}k_{\varphi 4\ell}E_4^+ & \mathrm{j}k_{\varphi 4\ell}E_4^- \\
-k_{M3\ell}^-E_3^+ & -k_{M3\ell}^-E_3^- & -k_{M4\ell}^-E_4^+ & -k_{M4\ell}^-E_4^- \\
\mathrm{j}k_{M3\ell}^-E_3^+ & \mathrm{j}k_{M3\ell}^-E_3^- & \mathrm{j}k_{M4\ell}^-E_4^+ & \mathrm{j}k_{M4\ell}^-E_4^- \\
-k_{Q3\ell}E_3^+ & k_{Q3\ell}E_3^- & -k_{Q4\ell}E_4^+ & k_{Q4\ell}E_4^- \\
-\mathrm{j}k_{Q3\ell}E_3^+ & \mathrm{j}k_{Q3\ell}E_3^- & -\mathrm{j}k_{Q4\ell}E_4^+ & \mathrm{j}k_{Q4\ell}E_4^-
\end{bmatrix}
\tag{23}
$$

with

$$
\begin{aligned}
E_\bullet^+ &= e^{\mathrm{j}\,\alpha_{\bullet\ell}z_\ell}, \qquad E_\bullet^- = e^{\mathrm{j}\,\alpha_{\bullet\ell}(L_\ell-z_\ell)}, \\
k_{\varphi\bullet\ell} &= \mathrm{j}\,\frac{\alpha_{\bullet\ell}^2 - \bar{\omega}_\ell^2\bar{E}_{0\ell} + \bar{d}_{a\ell}}{\alpha_{\bullet\ell}}, \\
k_{M\bullet\ell}^{\pm} &= E_{\pm\ell}^\star I_\ell\left(\alpha_{\bullet\ell}^2 - \bar{\omega}_\ell^2\bar{E}_{0\ell} + \bar{d}_{a\ell}\right), \\
k_{Q\bullet\ell} &= \mathrm{j}\,G_\ell^\star k_{S_\ell}A_\ell\left(\frac{-\bar{\omega}_\ell^2\bar{E}_{0\ell} + \bar{d}_{a\ell}}{\alpha_{\bullet\ell}}\right).
\end{aligned}
\tag{24}
$$

3.2. Assembly and solution procedure for the unbalance response

The solution $\tilde{\mathbf{x}}_{h\ell}^+(z_\ell)$ of each rotor segment is placed into the boundary and interface conditions. This leads to an equation system $\mathbf{Ac} = \mathbf{b}$ with the arbitrary constants $\mathbf{c} = [\mathbf{c}_1, \cdots, \mathbf{c}_\ell, \cdots, \mathbf{c}_M]^T$ of the homogenous solution. The rotor unbalance influences only the right-hand side vector $\mathbf{b}$. The solution of the linear equations system $\mathbf{Ac} = \mathbf{b}$ uniquely defines the state variables of the whole rotor. For a detailed explanation of the assembly procedure, the reader is referred to Klanner et al. [17].

3.3. Campbell diagram

The eigenvalues of a damped system are complex values and found by a recursive search algorithm presented in [19]. The imaginary part of the eigenvalues represents the whirl frequency, while the real part offers information about the stability of the system. The most common representation of the correlation between the spin speed and the whirl frequency is the Campbell diagram. In this diagram, the deviating lines from the horizontal indicate the forward and backward whirls. If the angular speed Ω of the rotor matches one of its natural frequencies ω, a critical speed of the rotor for an unbalance excitation is found.

4. NUMERICAL EXAMPLES

In this section, different examples of a general rotor-bearing system are presented. The examples are on one side modeled by a frequency-independent material model and on the other side with a frequency-dependent viscoelastic material model. Due to the variation of the different materials, which are used in the examples, the broad applicability of the fractional derivative material model and the used analytical computational technique is shown. All calculations are performed on an *Intel*® Core™ i7-10700 processor ($8 \times 2.90\,\text{GHz}$) with 32 GB RAM and a Windows 10 operating system. For the implementation of NAT, the software package *MATLAB*® *R*2021b has been used. The FEM model is also built in *MATLAB*® *R*2021b, for which the code of Friswell et al. [29] has been applied.

In Fig. 2 a rotating multi-stepped rotor-bearing system with homogenous circular cross-sections having the diameters $0.05\,\text{m}$ in segment 1, $0.06\,\text{m}$ in segments 2 and 7, $0.09\,\text{m}$ in segments 3 and 6, $0.11\,\text{m}$ in segment 4, and $0.14\,\text{m}$ in segment 5, is presented. The total length $L = 1\,\text{m}$ of the rotor is divided by $N = 8$ stations into $M = 7$ segments with the ratio of the rotor length to the maximum diameter is 7.1 and therefore the Timoshenko beam theory is applicable. Furthermore, the material of the rotor is steel with a density of $7800\,\text{kg/m}^3$. The total mass of the rotor is 55.85 kg. The external viscous damping coefficient in the x- and y-direction considering air as the ambient medium is given by $d_{a\ell} = 45\,\text{Ns/m}^2$.

In Case 1, the material parameters are given by the constant Young's modulus $E_\ell^c = 1.8 \cdot 10^{11}\,\text{N/m}^2$, and a shear modulus $G_\ell^c = 6.9 \cdot 10^{10}\,\text{N/m}^2$. The shear correction factor k_{S_ℓ} for the Timoshenko beam theory is assumed as 0.88.
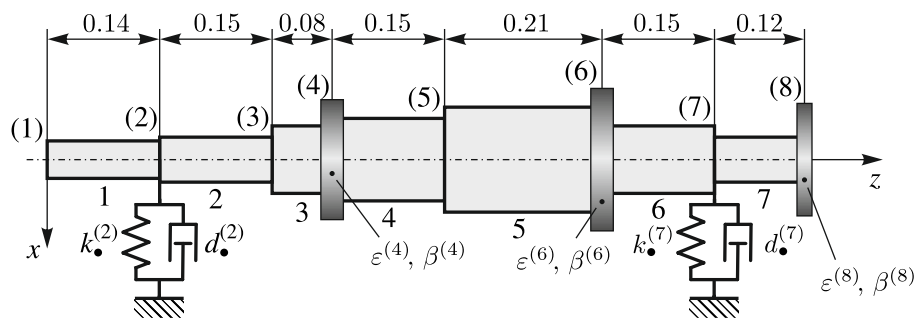
Fig. 2. Configuration of the example rotor

G. Überwimmer, G. Quinz, M. Klanner, and K. Ellermann

In Case 2, the material is described by a Kelvin-Voigt damping model with $E_\ell^{KV} = 1.8 \cdot 10^{11}\,\text{N/m}^2 \cdot (1 + \eta\,\text{j}\omega)$ and the parameter $\eta = 0.0203$.

In Case 3, the material is described by a fractional derivative damping. The parameters for the complex Young's modulus $E_{\pm\ell}^\star$ are given by $a_{0\ell}^E = 1.8 \cdot 10^{11}\,\text{N/m}^2$, $a_{1\ell}^E = 3.6589 \cdot 10^9\,\text{Ns}^{\alpha_\ell^E}/\text{m}^2$, and $\alpha_\ell^E = 0.63$, which have been given by Caputo and Mainardi [30]. The material in this example is isotropic with a Poisson's ratio $\nu_\ell = 0.3$.

In Case 4, all material parameters are the same as those in Case 3, except for the variable α_ℓ^E, which takes on values of $[0.2, 0.4, 0.6, 0.8]$.

In stations (2) and (7), the bearings of the rotor are modeled as a combination of linear springs and dampers. Additional rigid circular discs with negligible thickness are mounted in stations (4), (6), and (8). In Table 1 the parameters of the concentrated elements at the stations are specified.

The shaft is free of any unbalance and the occurring unbalance is concentrated at the rigid discs, according to Table 2.

To present the accuracy of NAT, the simulation is compared with a FEM model built with the Friswell code using small elements of 0.01 m for Case 1 and Case 2.

In Fig. 3a and Fig. 3b, the Campbell diagram of the different cases is presented.

A very good agreement between NAT and FEM for Case 1 and Case 2 is observed. The results using the fractional derivative damping models show a difference in the critical speeds and modes of the rotor. Due to the fractional exponent α_ℓ^E the rotor-bearing system reaches the modes at a smaller frequency compared to Case 2. The stability limit of Case 3 can be seen in Fig. 3b, where it is marked by a red cross. Due to the given external damping of the system, the stability limit of the fourth mode is reached only at high spin speeds. All other modes are stable for the investigated spin speed range.

(a) Case 1 and Case 2

(b) Case 2 and Case 3

Fig. 3. Campbell diagram

6

Bull. Pol. Acad. Sci. Tech. Sci., vol. 71, no. 6, p. e148610, 2023
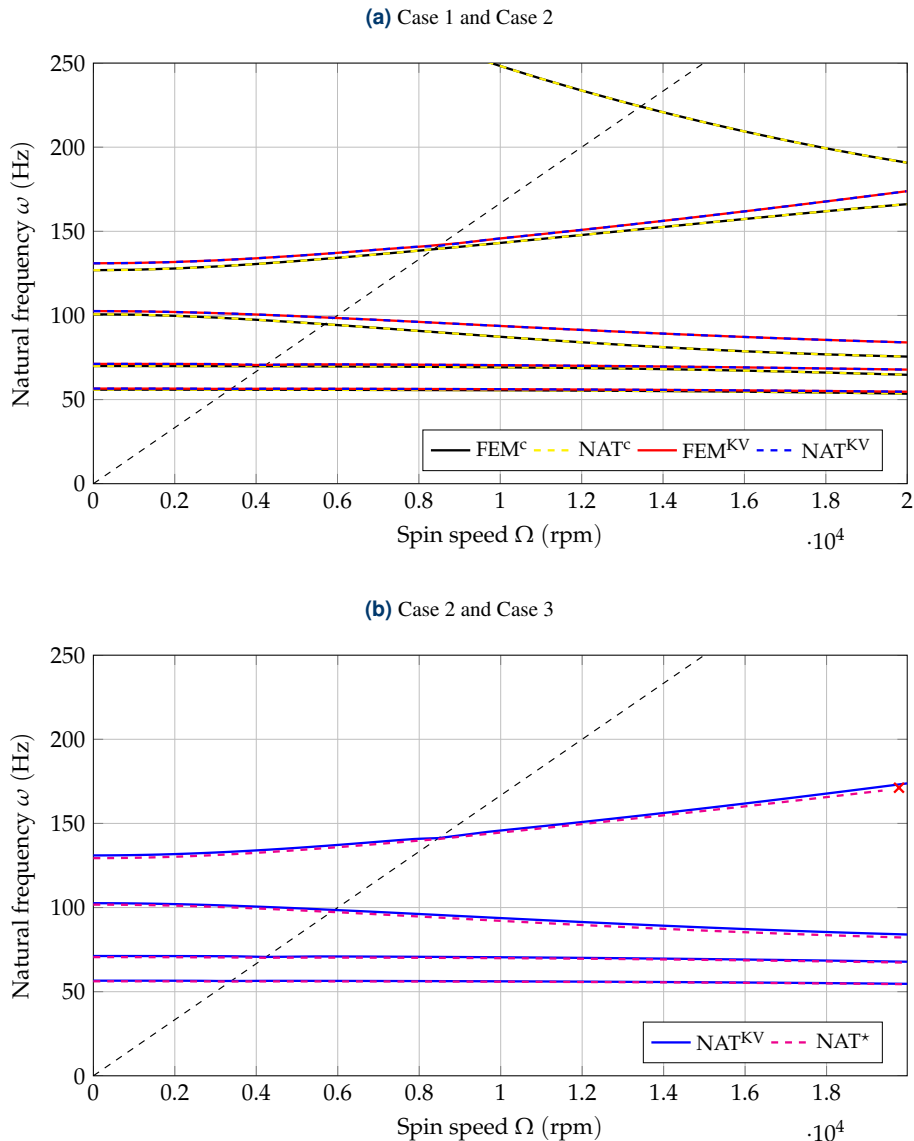
Numerical investigation of fractionally-damped rotor systems

Table 1
Parameters of the bearings and discs at the stations

(i)	Z_i (m)	$m^{(i)}$ (kg)	$\Theta_t^{(i)}$ (kg m²)	$\Theta_p^{(i)}$ (kg m²)	$k_{txx}^{(i)}$ (N/m)	$k_{tyy}^{(i)}$ (N/m)	$k_{txy}^{(i)}=k_{tyx}^{(i)}$ (N/m)	$d_{txx}^{(i)}=d_{tyy}^{(i)}$ (Ns/m)
1	0.00	–	–	–	–	–	–	–
2	0.14	–	–	–	$8\cdot10^6$	$5\cdot10^6$	$5\cdot10^5$	100
3	0.29	–	–	–	–	–	–	–
4	0.37	2.0	0.06	0.12	–	–	–	–
5	0.52	–	–	–	–	–	–	–
6	0.73	2.5	0.20	0.40	–	–	–	–
7	0.88	–	–	–	$6\cdot10^6$	$4\cdot10^6$	$5\cdot10^5$	100
8	1.00	1.5	0.15	0.30	–	–	–	–

Table 2
Unbalance of the rotor

(i)	Z_i (m)	U (kg m)	β (rad)
4	0.37	$4.0\cdot10^{-3}$	0
6	0.73	$1.0\cdot10^{-3}$	1.5
8	1.00	$3.6\cdot10^{-3}$	2.5

As shown in Table 3 and Fig. 3a the differences between the calculations with NAT and FEM of the same material model are negligible. The fractional derivative material model leads to critical speeds of $[56.04, 70.13, 97.40, 140.60]$ Hz.

A comparison of the unbalance response with different material models is shown in Fig. 4a for Case 1 and Case 2 and in Fig. 4b for Case 2 and Case 3. The parameter a denotes the major axis of the elliptical whirling orbit at an arbitrary position $z = 0.37$m. The evaluation by NAT fits perfectly with the result of FEM in Case 1 and Case 2 as shown in Fig. 4a.

Case 2 and Case 3 depict a general reduction of mode 5 as shown in Fig. 4b. In Case 3, where the fractional derivative material model is applied, a reduction of all occurring mode amplitudes is observed.

For Case 4, the influence of different values of α_ℓ^E on the rotor response is shown in Table 4. Therefore, the critical speeds

(a) Case 1 and Case 2

(b) Case 2 and Case 3
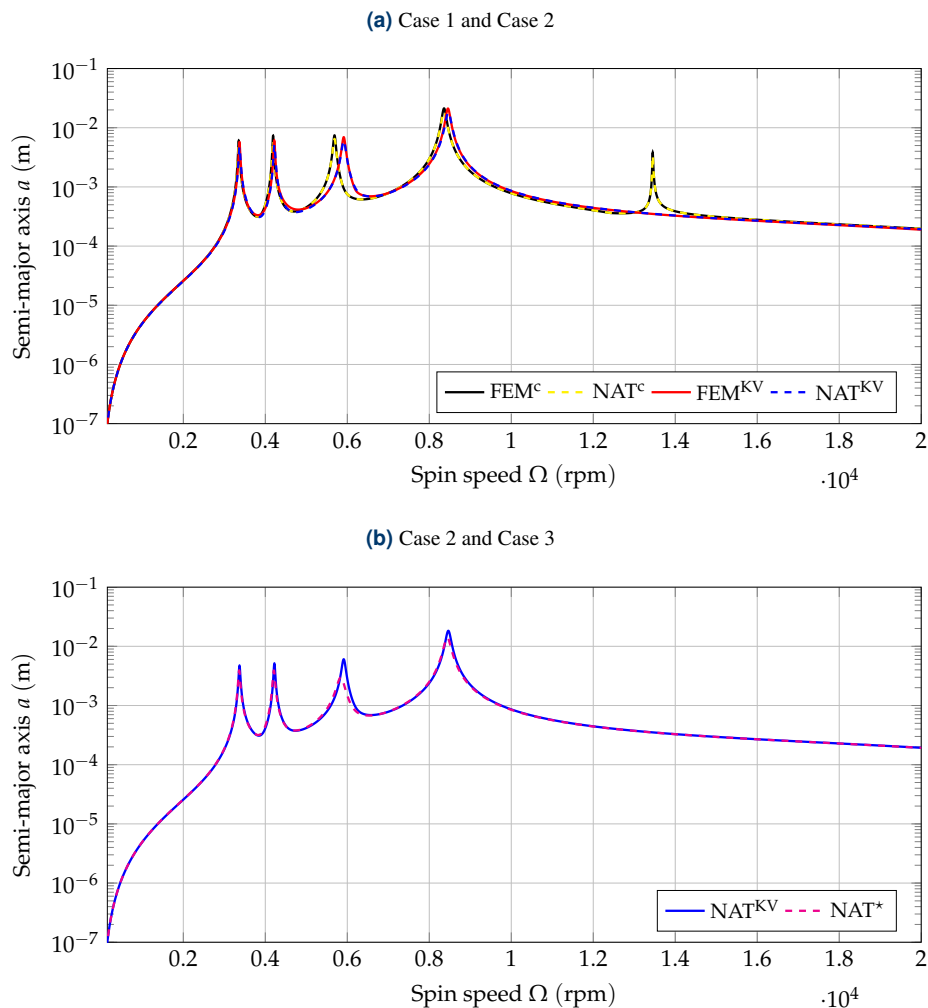
Fig. 4. Comparison of the unbalance response

Table 3
Critical speeds of the rotor

FEM (Hz)	NAT (Hz)	Relative Error NAT-FEM	FEM^{KV} (Hz)	NAT^{KV} (Hz)	Relative Error NAT^{KV} – FEM^{KV}
55.87	55.87	0.0035%	56.39	56.48	0.1011%
69.83	69.83	0.0003%	70.63	70.96	0.4545%
94.81	94.80	0.0045%	98.56	98.57	0.0132%
139.33	139.33	0.0013%	141.96	142.51	0.3867%
224.15	224.15	0.0002%			

and displacements of the semi-major axis of the first five critical speeds are compared, as presented in Table 4. This comparison involves determining the displacement of the semi-major axis of the elliptical whirling orbit at every point of the rotor with an increment of 0.01m at the critical speeds. Subsequently, the

Table 4
Critical speeds and average displacements semi-major axis with different α_ℓ^E

α_ℓ^E		Mode 1	Mode 2	Mode 3	Mode 4	Mode 5
0.2	ω (Hz)	55.85	69.80	94.85	139.28	225.62
	a (m)	0.0058	0.0071	0.0063	0.0199	0.0015
0.4	ω (Hz)	55.83	69.73	95.03	139.17	233.83
	a (m)	0.0064	0.0094	0.0054	0.0238	0.0005
0.6	ω (Hz)	55.80	69.60	95.62	138.88	260.53
	a (m)	0.0129	0.0183	0.0044	0.1390	0.0004
0.8	ω (Hz)	55.82	69.38	96.32	138.13	292.70
	a (m)	0.0046	0.0017	0.0057	0.0044	0.0004
1.0	ω (Hz)	56.80	68.85	96.72	136.77	315.62
	a (m)	0.0012	0.0007	0.0145	0.0011	0.0003

computed values are averaged and analysed. For the first four critical speeds the rotor itself is hardly deformed and the rotor displacement depends on the stiffness and damping properties of the bearings. For the fifth critical speed the material model becomes significant, since rotor deformation appears. In Fig. 5a the value of $\frac{|E^\star|}{a_{0\ell}^E} = 1 + \frac{a_{1\ell}^E}{a_{0\ell}^E}|(\mathrm{j}\omega)^{\alpha_\ell^E}|$, which describes the increase of the rotor stiffness due to higher values of α_ℓ^E, are shown over the observed frequency range. The points of the critical speeds are denoted by crosses. It is apparent that the stiffness increases with higher values of α_ℓ^E, which is consistent with the rising critical speeds shown in Table 4. The resulting loss factor of the Kelvin-Voigt material model within the considered spin speeds is illustrated in Fig. 5b. As expected the loss factor increases with rising frequency, which is less pronounced for lower α_ℓ^E. Therefore, the deformation at the fifth critical speed is lower for increasing α_ℓ^E. The selection of α_ℓ^E determines the slope of the stiffness increase and loss factor, and allows for an accurate modelling of the material behaviour in a limited frequency range.

5. CONCLUSIONS

In this paper, an extension of NAT has been made. Therefore, the rotating Timoshenko beam with a fractional derivative material damping model has been solved analytically. With the efficient way of NAT, the rotor-bearing systems are investigated and the accuracy of NAT has been shown in numerical examples. Furthermore, the effects of a fractional derivative material damping model have been presented and the influence on higher spin speeds has been discussed. As long as the rotor is driven with low spin speeds, the material model has nearly no influence on the modes. If a high spin speed rotor is considered, the material model is gaining more importance for a better understanding of the rotor-bearing systems real behaviour. Therefore, a classical model may not be sufficient and could be replaced by a fractional derivative material model.

(a) Stiffness increase for different α_ℓ^E

(b) η for different α_ℓ^E
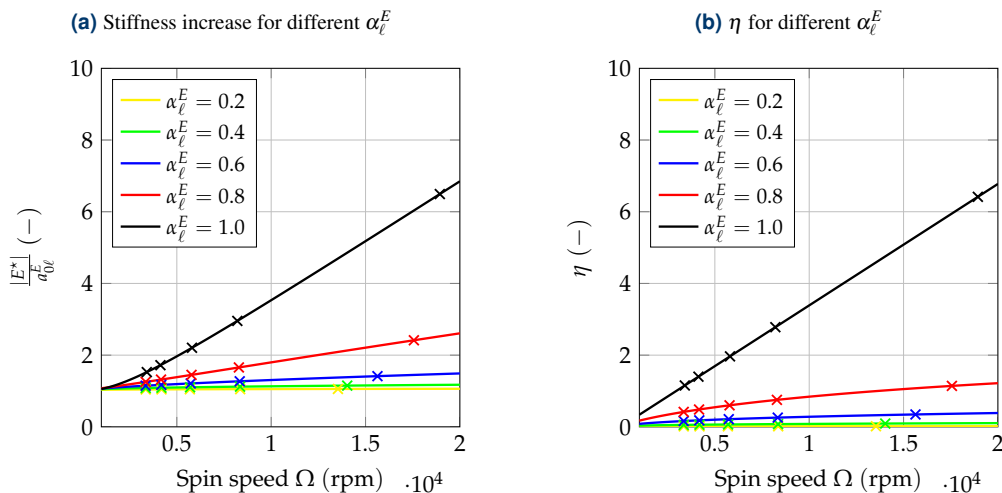
Fig. 5. Material parameter for different α_ℓ^E

8

Bull. Pol. Acad. Sci. Tech. Sci., vol. 71, no. 6, p. e148610, 2023

REFERENCES

[1] M. Klanner, M. Prem, and K. Ellermann, "Quasi-analytical solutions for the whirling motion of multi-stepped rotors with arbitrarily distributed mass unbalance running in anisotropic linear bearings," *Bull. Pol. Acad. Sci. Tech. Sci.*, vol. 69, no. 6, p. e138999, Dec 2021, doi: 10.24425/bpasts.2021.138999.

[2] P. Nutting, "A new general law of deformation," *J. Frankl. Inst.*, vol. 191, no. 5, pp. 679–685, May 1921, doi: 10.1016/s0016-0032(21)90171-6.

[3] T. Pritz, "Analysis of four-parameter fractional derivative model of real solid materials," *J. Sound Vibr.*, vol. 195, no. 1, pp. 103–115, Aug 1996, doi: 10.1006/jsvi.1996.0406.

[4] A. Labuschagne, N. van Rensburg, and A. van der Merwe, "Comparison of linear beam theories," *Math. Comput. Model.*, vol. 49, no. 1-2, pp. 20–30, Jan 2009, doi: 10.1016/j.mcm.2008.06.006.

[5] P. Ruge and C. Birk, "A comparison of infinite Timoshenko and Euler–Bernoulli beam models on winkler foundation in the frequency- and time-domain," *J. Sound Vibr.*, vol. 304, no. 3-5, pp. 932–947, Jul 2007, doi: 10.1016/j.jsv.2007.04.001.

[6] R. Tamrakar and N. Mittal, "Modal behaviour of rotor considering rotary inertia and shear effects," *Persp. Sci.*, vol. 8, pp. 87–89, Sep 2016, doi: 10.1016/j.pisc.2016.04.003.

[7] E. S. Zorzi and H. D. Nelson, "Finite element simulation of rotor-bearing systems with internal damping," *J. Eng. Power*, vol. 99, pp. 71–76, 1977.

[8] G. Genta, "On a persistent misunderstanding of the role of hysteretic damping in rotordynamics," *J. Vib. Acoust.*, vol. 126, no. 3, pp. 459–461, Jul 2004, doi: 10.1115/1.1759694.

[9] K. Baumann, E. Bopple, R. Markert, and W. Schwarz, "Einfluss der inneren Dämpfung auf das dynamische Verhalten von elastischen Rotoren," *VDI Berichte*, no. 2003, pp. 55–69, 2007.

[10] H.D. Nelson, "A finite rotating shaft element using timoshenko beam theory," *J. Mech. Des.*, vol. 102, no. 4, pp. 793–803, Oct 1980, doi: 10.1115/1.3254824.

[11] H. N. Özgüven and Z. Özkan, "Whirl speeds and unbalance response of multibearing rotors using finite elements," *J. Vib. Acoust.-Trans. ASME*, vol. 106, pp. 72–79, 1984.

[12] M.A. Prohl, "A general method for calculating critical speeds of flexible rotors," *J. Appl. Mech.*, vol. 12, no. 3, pp. A142–A148, Sep 1945, doi: 10.1115/1.4009455.

[13] A.-C. Lee, Y.-P. Shih, and Y. Kang, "Analysis of linear rotor-bearing systems. A general transfer matrix method," *J. Vib. Acoust.-Trans. ASME*, vol. 115, no. 4, pp. 490–497, Oct 1993.

[14] Y.-P. Shih and A.-C. Lee, "Identification of the unbalance distribution in flexible rotors," *Int. J. Mech. Sci.*, vol. 39, pp. 841–857, 1997.

[15] O. Özşahin, H. Özgüven, and E. Budak, "Analytical modeling of asymmetric multi-segment rotor – bearing systems with timoshenko beam model including gyroscopic moments," *Comput. Struct.*, vol. 144, pp. 119–126, Nov 2014, doi: 10.1016/j.compstruc.2014.08.001.

[16] J.-S. Wu and H.-M. Chou, "A new approach for determining the natural frequencies and mode shapes of a uniform beam carrying any number of sprung masses," *J. Sound Vibr.*, vol. 220, no. 3, pp. 451–468, Feb 1999, doi: 10.1006/jsvi.1998.1958.

[17] M. Klanner, M. Prem, and K. Ellermann, "Steady-state harmonic vibrations of a linear rotor-bearing system with a discontinuous shaft and arbitrarily distributed mass unbalance," in *Proceedings of ISMA 2020 International Conference on Noise and Vibration Engineering and USD2020 International Conference on Uncertainty in Structural Dynamics*, Oct 2020, pp. 1257–1272.

[18] G. Quinz, M. Prem, M. Klanner, and K. Ellermann, "Balancing of a linear elastic rotor-bearing system with arbitrarily distributed unbalance using the numerical assembly technique," *Bull. Pol. Acad. Sci. Tech. Sci.*, vol. 69, no. 6, p. e138237, Dec 2021, doi: 10.24425/bpasts.2021.138237.

[19] G. Quinz, M. Klanner, and K. Ellermann, "Balancing of flexible rotors supported on fluid film bearings by means of influence coefficients calculated by the numerical assembly technique," *Energies*, vol. 15, no. 6, pp. 1–18, Mar 2022, doi: 10.3390/en15062009.

[20] G. Quinz, M. Klanner, and K. Ellermann, "Balancing of rotor-bearing systems without trial runs using the numerical assembly technique – an experimental investigation," in *Proceedings of ISMA 2022 International Conference on Noise and Vibration Engineering and USD2022 International Conference on Uncertainty in Structural Dynamics*, Sep 2022, pp. 1542–1553.

[21] G. Quinz, G. Überwimmer, M. Klanner, and K. Ellermann, "Field balancing of flexible rotors without trial runs using the numerical assembly technique," in *Proceedings of the SIRM2023: 15th European Conference on Rotordynamics*, Feb 2023.

[22] R.L. Bagley and P.J. Torvik, "A theoretical basis for the application of fractional calculus to viscoelasticity," *J. Rheol.*, vol. 27, no. 3, pp. 201–210, Jun 1983, doi: 10.1122/1.549724.

[23] M. Caputo and F. Mainardi, "A new dissipation model based on memory mechanism," *Pure Appl. Geophys. PAGEOPH*, vol. 91, no. 1, pp. 134–147, 1971, doi: 10.1007/bf00879562.

[24] M. Caputo, "Linear models of dissipation whose q is almost frequency independent – II," *Geophys. J. Int.*, vol. 13, no. 5, pp. 529–539, Nov 1967, doi: 10.1111/j.1365-246x.1967.tb02303.x.

[25] K. Singh, R. Saxena, and S. Kumar, "Caputo-based fractional derivative in fractional fourier transform domain," *IEEE J. Emerg. Sel. Top. Circuits Syst.*, vol. 3, no. 3, pp. 330–337, Sep 2013, doi: 10.1109/jetcas.2013.2272837.

[26] G. Genta, *Dynamics of Rotating Systems*. Springer-Verlag, 2005, doi: 10.1007/0-387-28687-x.

[27] O.A. Bauchau and J.I. Craig, *Structural Analysis*. Springer-Verlag GmbH, Aug 2009.

[28] P. Hagedorn and A. DasGupta, *Vibrations and Waves in Continuous Mechanical Systems*. John Wiley & Sons, 2007.

[29] M.I. Friswell, J.E.T. Penny, S.D. Garvey, and A.W. Lees, *Dynamics of Rotating Machines*. Cambridge University Press, Mar 2010, doi: 10.1017/cbo9780511780509.

[30] M. Caputo and F. Mainardi, "Linear models of dissipation in anelastic solids," *La Rivista del Nuovo Cimento*, vol. 1, no. 2, pp. 161–198, Apr 1971, doi: 10.1007/bf02820620.

Bull. Pol. Acad. Sci. Tech. Sci., vol. 71, no. 6, p. e148610, 2023

9